JOURNAL OF PROPULSION AND POWER
Vol. 12, No. 3, May–June 1996

Unsteady Pressure Behavior in a Ramjet/Scramjet Inlet

Patrick E. Rodi*
National Research Council, Hampton, Virginia 23681
Saied Emami†
Lockheed Engineering and Sciences Company, Inc., Hampton, Virginia 23681
and
Carl A. Trexler‡
NASA Langley Research Center, Hampton, Virginia 23681

Mean and time-accurate pressures have been measured in the inlet of a dual-mode, ramjet/scramjet configuration. This configuration was designed for low hypersonic Mach number operation using a hydrocarbon-based fuel. The time-accurate measurements are presented for inlets operating at maximum permissible back-pressure during and after inlet unstart.

Nomenclature

f = frequency, Hz
G = power spectral density
M_1 = freestream Mach number
P = mean wall pressure
P_t = tunnel total pressure
P_1 = freestream static pressure
p = time accurate static wall pressure
$\bar{p}$ = average of the time accurate pressure data
R_{ii} = autocorrelation for gauge i
T_t = tunnel total temperature
X = longitudinal distance measured from the inlet leading edge
Y = vertical distance measured from the inlet leading edge
δ = flow turning angle, deg
σ = standard deviation of wall static pressure data

Introduction

HIGH Mach number air-breathing propulsion systems, for vehicles such as the National Aerospace Plane (X-30), generally focus upon highly integrated supersonic combustion ramjets (scramjets). The air-breathing propulsion performance, airframe structural integrity, and system cooling requirements of such vehicles generally dictate the use of cryogenic hydrogen fuel.[1] However, for missions at and below Mach 8, such as for hypersonic cruise missiles, a hydrocarbon-based fuel is attractive because of its high density and ease of storage and handling.[2]

The concept of an engine designed to operate with both subsonic and supersonic combustion (i.e., dual-mode) has existed for many years.[3] A number of studies have investigated this concept and a recent presentation of dual-mode engine theory and design are presented in Refs. 4 and 5, respectively.

In the current investigation, time-accurate pressures, measured at a number of locations within an inlet designed for a hydrocarbon-fueled, dual-mode engine, are analyzed using standard time series techniques. The objectives are 1) to study the instantaneous pressure behavior within a dual-mode inlet operating at maximum back pressure and after inlet unstart; 2) to study the transients occurring during back-pressure-induced inlet unstarts; 3) to compare the behavior between a back-pressure-induced unstart (BPIU) and a cowl-induced unstart (CIU) (i.e., contraction ratio induced); and 4) to further understand the controlling physics of inlet unstarts.

Received Dec. 18, 1994; revision received Dec. 20, 1994; presented as Paper 95-0037 at the AIAA 33rd Aerospace Sciences Meeting and Exhibit, Reno, NV, Jan. 9–12, 1995; accepted for publication Jan. 9, 1996. This paper is declared a work of the U.S. Government and is not subject to copyright protection in the United States.

*Resident Research Associate, NASA Langley Research Center, Gas Dynamics Division (HAPB), M/S 168. Member AIAA.
†Principal Engineer, NASA Langley Research Center, M/S 168.
‡Aerospace Research Engineer, Gas Dynamics Division (HAPB), M/S 168.

Experimental Configuration

Test Facility and Test Conditions

The NASA Langley Mach 4 Blow Down Facility (M4BDF) was used for these experiments. The test section is nominally 9 × 9 in. (22.9 × 22.9 cm) square in cross section, and 35 in. (89.0 cm) in length. The two-dimensional, fixed-geometry facility nozzle produces airflow at steady conditions to the test section for a nominal test time of 2.0 min. Calibration of the M4BDF (unpublished data) revealed a nozzle core flow Mach number of 4.03 ± 0.02. Dry, unheated air was the test gas at a nominal freestream total pressure of 200 ± 2 psia (1.38 MPa). At these conditions, the tunnel freestream static pressure P_1 in the test section is 1.266 ± 0.034 psia (60 Pa). The total temperature in this unheated tunnel varied slightly between runs, but was approximately 530 ± 5°R (294 K), producing a nominal freestream Reynolds number of 20.3 × 10^6/ft (66.6 × 10^6/m). The inlet model was initially at ambient temperature. These thermal conditions produced a moderately warm wall condition with an actual wall temperature to adiabatic wall temperature ratio of T_w/T_{aw} = 1.11.

Test Model

The two-dimensional planar inlet model, shown in Fig. 1 (the inlet combined with combustor–nozzle section of a proposed hydrocarbon-fueled engine) and in Fig. 2 (an enlarged view of the inlet section), was made of aluminum and was 28.89 in. (73.38 cm) long and 2.03 in. (5.16 cm) wide. The initial bodyside (lower side) ramp-turning angle of the inlet was 5 deg with additional compression corners of 3 and 4 deg located at X = 5.81 and 10.98 in. (14.76 and 27.89 cm). The inlet contraction ratio could be changed by adjusting a movable cowl. The cowl, fitted opposite the bodyside compression surface, was designed to pivot about the inlet/isolator junction (i.e., inlet throat). This cowl was 4.00 in. (10.16 cm) in length and could be rotated from +6 deg (away from the bodyside) to −8 deg (toward the bodyside), measured relative to the freestream direction. Downstream of the inlet a 1.32-in.- (3.35-cm-) long constant-area section (i.e., isolator) was included

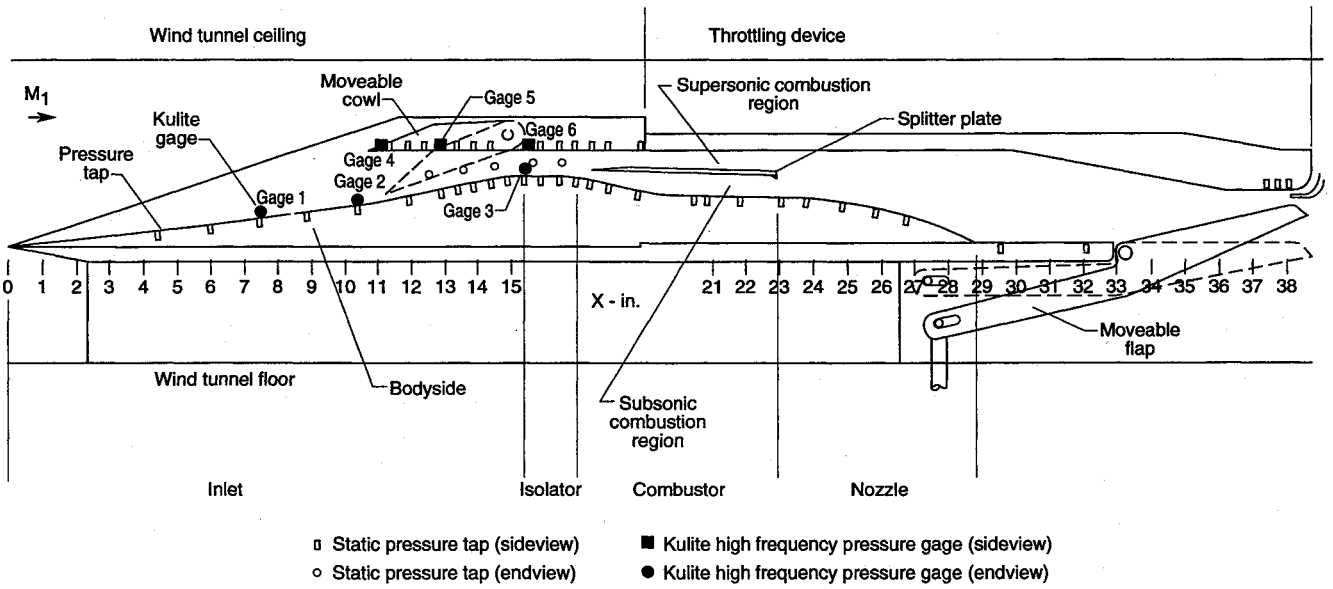

Fig. 1 Dual-mode, hydrocarbon-fueled engine model.

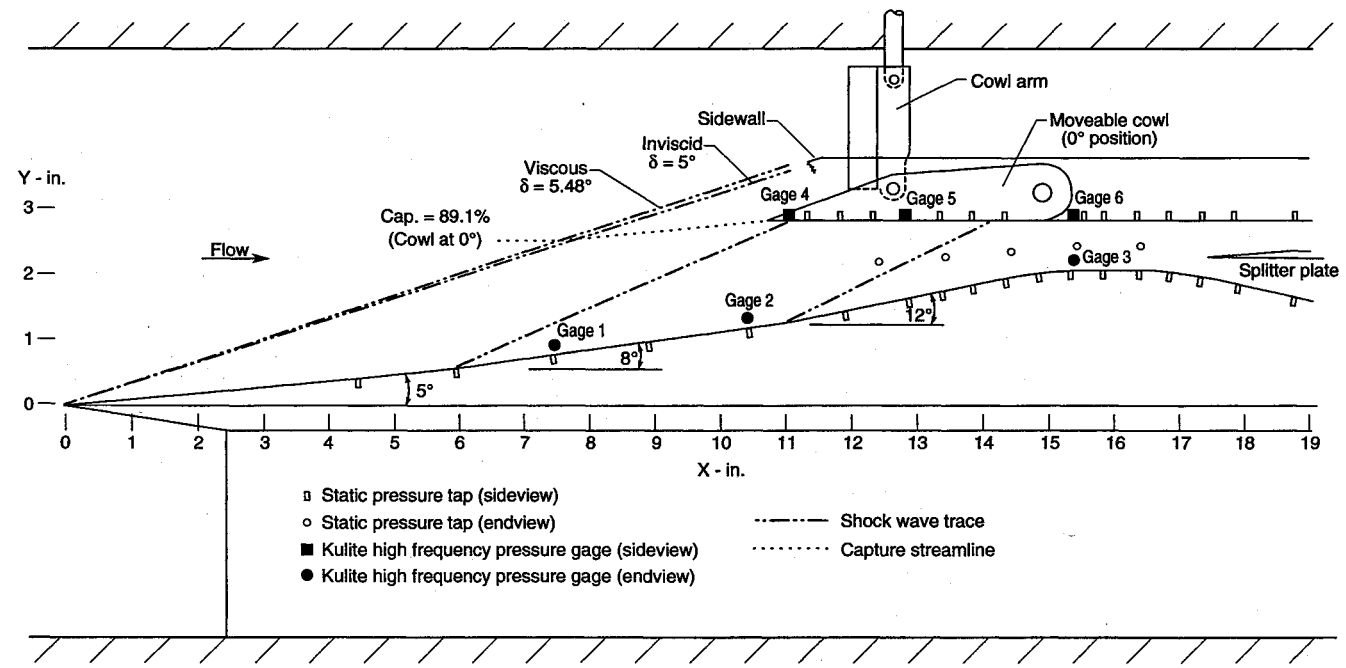

Fig. 2 Close-up of inlet portion of the wind-tunnel model.

between the inlet and the combustor section. The expansion at the inlet throat was a constant radius curve of radius 6.680 in. (16.97 cm) tangent to the compression face at X = 14.16 in. (35.97 cm) and tangent to the isolator section at X = 15.55 in. (39.50 cm). The combustor section was divided into a scramjet portion (on the cowl side) and a ramjet portion (on the bodyside). Sixty-eight static pressure orifices (0.040 in. i.d.) were installed in axial and spanwise rows throughout the model, as shown in Fig. 1. Six dynamic pressure (Kulite®) gauges, mounted flush with the model wetted surfaces, were located within the inlet and at the inlet/isolator junction of the model, as shown in Figs. 1 and 2. Gauges 1–3 were located along one sidewall of the model, immediately adjacent to the sidewall/bodyside junction. Gauges 4–6 were installed on the cowl at 0.35 in. (0.89 cm) off the centerline of the model cowl, or 0.65 in. (1.65 cm) away from the side wall. The explicit locations of the six dynamic pressure gauges with respect to the X (axial) and Y (vertical) coordinate system, measured from the model leading edge, are 7.49 in., 0.9 in. (19.02 cm, 2.29 cm); 10.44 in., 1.33 in. (26.52 cm, 3.38 cm); 15.39 in., 2.24 in. (39.10 cm, 5.69 cm); 11.10 in., 2.83 in. (28.19 cm, 7.19 cm); 12.85 in., 2.83 in. (32.64 cm, 7.19 cm); and 15.36 in., 2.83 in. (39.01 cm, 7.19 cm) for gauges 1–6, respectively.

A throttling device was attached to the downstream end of the model. The device's exit area could be decreased during a run, gradually forcing a shock train upstream into the model to simulate the increased inlet back-pressure associated with combustion.

The inlet contraction ratio and mass capture were calculated using the geometric properties of each inlet configuration and assuming a two-dimensional flowfield. Using these assumptions, and the oblique shock relations, the captured streamtube was determined for each configuration. The contraction ratio is defined as the ratio of the initial cross-sectional area of the captured streamtube to the throat area of the inlet. The mass capture values are expressed as a percentage of the mass flow through the projected frontal area of the inlet (i.e., the product of the inlet width and the inlet height measured from the be-

Table 1 Inlet configurations and mass capture

Cowl angle, deg	Contraction ratio	Mass capture, %
−8	1.99	69.2
−4	2.62	80.9
0	3.23	89.1
+2	3.51	92.1
+4	3.77	94.4
+6	4.04	96.5

ginning of the bodyside ramp to the leading edge of the cowl). These quantities are tabulated in Table 1.

Data Acquisition

The principal objective of this study was to obtain test data that are descriptive of the performance of inlet/isolator and isolator/combustor combinations that are representative of dual-mode scramjets. Test duration was 2 min; during this time, either the cowl angle or the throttling device exit was remotely actuated. Measurements include mean and time-accurate surface pressures. The mean pressure measurements were obtained using conventional surface pressure taps connected to four electronically scanned pressure (ESP) modules. The measurement uncertainty for the pressure data was ±0.02 psia or ±0.03% of measurement, whichever was greater. The model pressure data were measured by a separate data-acquisition/buffer system and then transferred to the first of two personal computers used for data acquisition. This personal computer was also used to measure four additional channels for tunnel stagnation conditions and the throttling device position through an onboard analog-to-digital (A/D) converter. These data were integrated with the ESP pressure measurements after every run. All of these data channels were sampled at 1 Hz. A single measurement sweep across all of the data channels is referred to as a cycle. Thus, 120 cycles of data were obtained within the 2 min of testing.

A second personal computer was used to sample the time-accurate pressure signals from the six Kulite 0–30 psia dynamic pressure transducers. These transducers were calibrated at NASA Langley to an accuracy of ±0.17 psia (±1180 Pa). The output signals of these gauges were amplified and filtered using a low-pass filter set to 10 kHz and then sampled at 20 kHz using a high-speed A/D converter. The data were acquired concurrently on each channel by using a sample and hold circuit. The time-accurate data were acquired for a 10-s (200,000 points) interval to ensure capture of the inlet unstart and provide statistically meaningful results of the pressure signals before and after the unstart. The effective bandwidth for a Fourier transform of random data is the sampling frequency divided by twice the number of points in the data frame. Thus, the effective bandwidth value is 4.88 Hz for all analyses presented in this article.

Results and Discussion

The unfueled performance of a similarly shaped dual-mode engine was reported by Andrews et al.[6] Their paper focused on the simulated operation of the ramjet/scramjet combustor section and the effects on performance from various geometrical perturbations of combustor flowpath with a fixed, low contraction ratio, self-starting inlet. However, the current test program utilized a variable contraction ratio inlet and focused on the time-accurate behavior of the pressure field before, during, and after inlet unstart. Large-scale flowfield fluctuations can have serious ramifications in such areas as vehicle stability and control, high instantaneous structural loading, and fatigue of the aircraft structure. The unsteadiness can also have a large effect on flowfield uniformity entering the combustor and on the time-dependent behavior of the combustion process itself. In this study, time-accurate data were acquired at various cowl angles from +6 to −8 deg. The time-accurate measurements were analyzed using conventional time series analysis techniques.[7,8]

Pressure Behavior Caused by Back-Pressure-Induced Unstarts

In general, high contraction ratio inlets are not self-starting at low Mach numbers. To study back-pressure-induced unstarts for various inlet contraction ratios, a method was needed to ensure inlet starting at the beginning of each run. To aid in inlet starting, the cowl was rotated to a low contraction ratio position (e.g., −8 deg), before the tunnel was started. Once the airflow had been established and the tunnel and model were started, the cowl was repositioned to the desired cowl angle.

The maximum permissible back-pressure that an inlet can sustain prior to unstarting determines the amount of fuel that can be burned within a given combustor area and, consequently, the amount of thrust the engine can produce. For greatest thrust production, the permissible back-pressure should be as high as possible. Emami et al.[9] demonstrated that the amount of maximum sustainable combustor pressure threshold, which an inlet can withstand before the onset of the inlet unstart (i.e., the maximum back-pressure limit), depends upon the incoming flow conditions, inlet geometry, contraction ratio, and isolator length. In the current unfueled tests, the throttling device (Fig. 1), located downstream of the model, was used to increase the inlet back-pressure. As the exit area of the throttling device was reduced, a shock train was forced into the model. The resulting pressure increase simulated the pressure increase because of combustion. Figure 3 shows the mean pressure distributions on the bodyside of the model as the back-pressure is incrementally increased, (curves no. 1–4), for the +6-deg cowl configuration. Note that the increased pressure level occurs initially at the downstream region of the model and gradually moves further upstream as the back-pressure is increased. Just before unstart, the inlet reaches the maximum permissible back-pressure (curve no. 4). Any further decrease in throat height of the throttling device causes the inlet to unstart (curve no. 5). The pressure increase observed ahead of the cowl for the unstarted condition is a result of the detached shock system characteristic of unstarted inlets. This system permits much of the air to spill around the inlet, substantially reducing the captured mass flow and causing a major redistribution of the pressure field.

The mean pressure distributions measured along the bodyside and cowl side of the inlet configurations at maximum back-pressure are plotted using open symbols in Figs. 4 and 5, respectively. The maximum pressure distributions plotted in Figs. 4 and 5 are analogous to curve no. 4 on Fig. 3. The average of the time-accurate measurements are also plotted

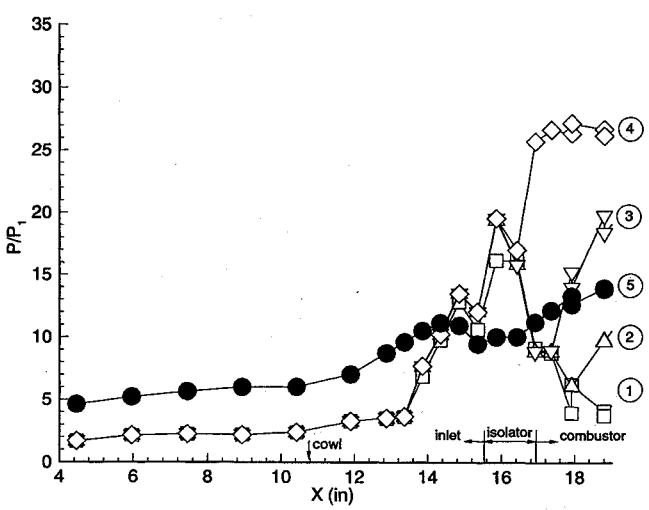

Fig. 3 Representative mean pressure distributions along the bodyside of the model during increased back-pressure.

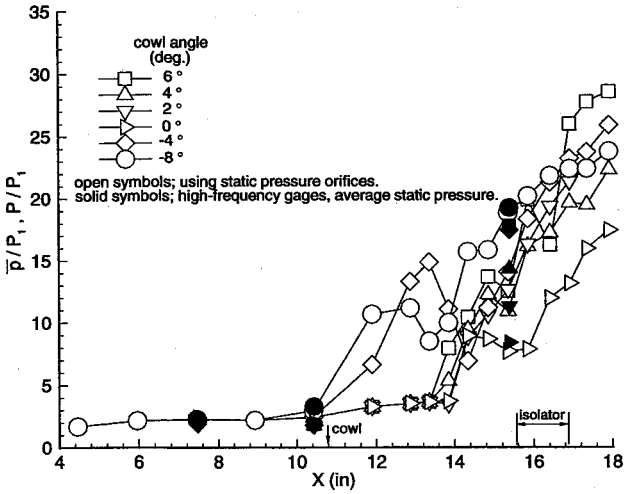

Fig. 4 Mean pressure distribution and average fluctuating pressures on the bodyside of the inlet for each configuration operating at maximum back-pressure.

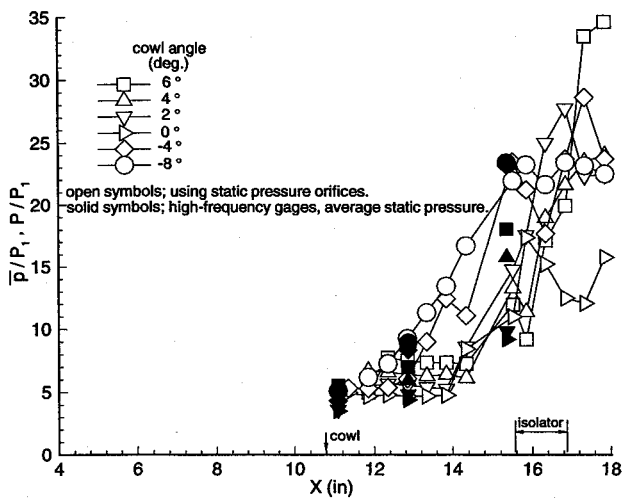

Fig. 5 Mean pressure distribution and average fluctuating pressures on the cowl side of the inlet for each configuration operating at maximum back-pressure.

using closed symbols. To minimize systematic errors, all test data were nondimensionalized by tunnel static pressure for each test run. Examination of the test data showed that the measurements were repeatable from run-to-run. Ahead of the inlet throat, the average values of the fluctuating pressure data agree with mean data obtained from the static pressure orifices on both the bodyside and cowl side of the model. However, in the throat region, the mean pressure data deviates from the average of the fluctuating measurements on both the bodyside and the cowl side. This deviation can be attributed to the highly three-dimensional flowfield resulting from the interaction of the cowl shock impinging on the bodyside near the inlet shoulder, the flow expansion beginning at the shoulder, and the influence from downstream back-pressure traveling upstream through the subsonic portions of the flow. The three-dimensional flowfields could produce spanwise variations in flow properties between the model centerline (where the pressure taps were located) and the corner region (where the high-frequency gauges were installed). Highly three-dimensional flowfields have been documented in similar configurations and back-pressure conditions by other investigators such as Reddy and Weir.[10]

Emami et al.[9] tested three two-dimensional planar supersonic inlets with the same inlet inflow conditions. The inlet geometries varied only in the length of the cowl. The test results showed that all three inlets unstarted at approximately the same convergence cowl angle independent of inlet cowl length, contraction ratio, and mass capture. This finding is an explicit indication of strong shock boundary-layer interactions in conjunction with the instability of a boundary layer growing toward a fully separated boundary layer throughout the entire inlet, which is the eventual cause of disgorging a terminal shock out the inlet. In addition, Reddy and Weir[10] buttressed the critical role of boundary-layer development specifically in a throat of a Mach 5 two-dimensional planar inlet using time-averaged three-dimensional numerical simulation in conjunction with experimental pitot tube pressure probe data.

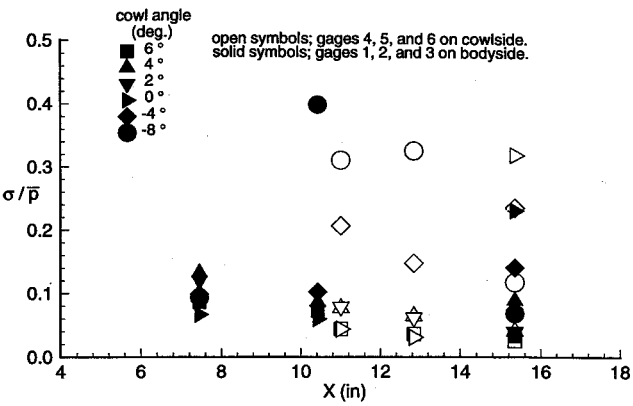

Fig. 6 Normalized standard deviation of the fluctuating pressure signals for each configuration operating at maximum back-pressure.

In this article, the high-frequency time-accurate pressure data were utilized to address the dynamic of the local boundary-layer separation in terms fluctuating pressure levels throughout the inlet, in addition to the corresponding interrelationships between those local fluctuating components for right before and after the inlet unstart. Realizing that the magnitude of fluctuating pressure varies for each configuration (Reynolds number dependent), all fluctuating data were nondimensionalized with respect to mean pressure (or average of time-accurate pressure) values to generalize the instability character and universal behavior of boundary-layer separation immediately before and after unstart.

For the time-accurate data, the standard deviation of the signal is used to quantify the degree of fluctuation observed. The standard deviation, when operating at the maximum back-pressure, normalized by the average of the signal is plotted vs streamwise position along the bodyside and cowl side of the inlet in Fig. 6. The large values of normalized standard deviation illustrate the large relative magnitude of the pressure fluctuations. For every configuration (except the −8-deg case), the normalized standard deviation for gauge no. 2 was less than that for gauge no. 1. This is possibly because of the proximity of gauge no. 1 to the compression corner located at $X = 5.81$ in. (14.76 cm). The strong pressure gradients located at the corner would tend to increase the fluctuation intensity. This has been seen in earlier investigations of compression corner induced shock wave/turbulent boundary-layer interactions.[11] The fluctuations relax somewhat downstream of the corner as gauge no. 2 is reached. For comparison, without back-pressure the standard deviation for gauges no. 1 and 2 (not shown in the figures) was roughly 5% of the average pressure value. This ratio is in agreement with earlier developed empirical correlations for the fluctuations under supersonic turbulent boundary layers.[12] The other gauges are located within the shock train induced by the throttling device and experience large scale fluctuations in pressure.

Transient Behavior During Back-Pressure-Induced Unstart

The pressure time histories during the back-pressure-induced unstart for the cowl at +6 deg are shown in Fig. 7. The

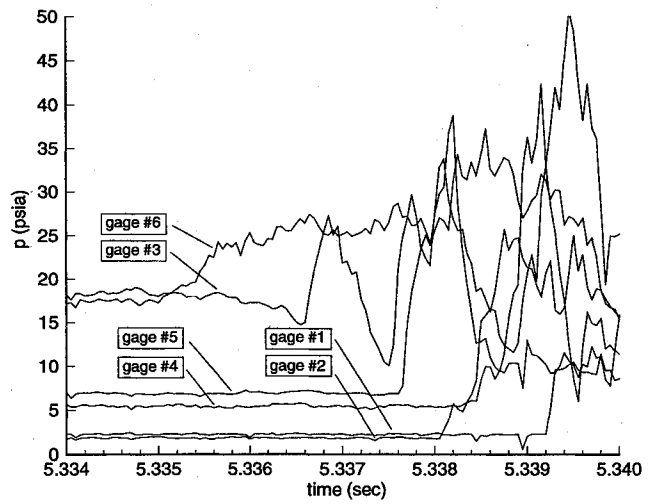

Fig. 7 Time pressure histories during the unstart transient for the +6-deg cowl configuration.

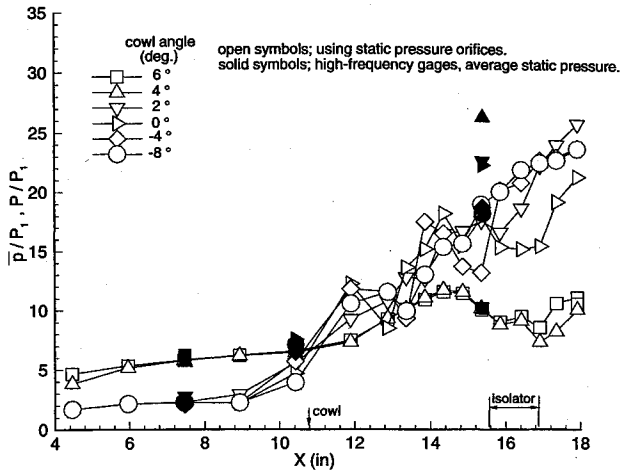

Fig. 8 Mean pressure distribution and average fluctuating pressures on the bodyside of the inlet for each configuration after back-pressure induced inlet unstart.

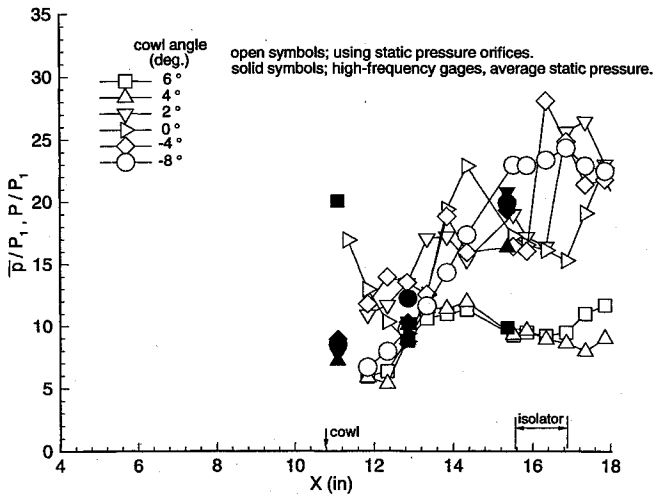

Fig. 9 Mean pressure distribution and average fluctuating pressures on the cowl side of the inlet for each configuration after back-pressure induced inlet unstart.

onset of inlet unstart is seen as a wave that translates from downstream to upstream through the inlet. By examining the times between the passage of this wave and knowing the distances between the gauges, the mean wave velocity can be calculated. Using gauges no. 1 and 2, on the bodyside of the inlet, the mean wave moves upstream at approximately 206 ± 12 ft/s (63 m/s). Along the cowl between gauges no. 4 and 5, the wave moves upstream at approximately 194 ± 12 ft/s (59 m/s). In every dataset where the onset of unstart can be clearly identified, the unstart transient appears as a wave moving from downstream to upstream at a velocity in the range from 182 to 230 ft/s (55 to 70 m/s). Similar high-speed pressure transients during inlet unstart have been studied earlier.[13]

Pressure Behavior After Back-Pressure-Induced Unstart

The mean pressure distributions measured along the bodyside and cowl side of the inlet configurations, after a back-pressure-induced unstart, are plotted using open symbols in Figs. 8 and 9, respectively. The average of the time-accurate measurements is also included on these figures using solid symbols. The most salient feature in these two figures, that differentiates one mean pressure distribution from another, is the distinct distribution shape for the two highest contraction ratio inlets (+6- and +4-deg cowl angles). These relatively flat distributions are characteristic of unstarted high contraction ratio, two-dimensional inlets, and are labeled a hard unstart. The other cases are representative of inlets that begin to vent a small amount of mass and gradually unstart. This is termed a soft unstart. As explained previously for the data at maximum back-pressure, the average of the time-accurate data after unstart may not agree with the mean pressure data because of the different spanwise locations of the gauges and the static taps.

The average and standard deviations of the time-accurate pressure data were also calculated after unstart. The normalized standard-deviation values are plotted in Fig. 10 for the bodyside and cowl side of the model after unstart. Figure 10 can be compared with the data discussed previously in Fig. 6 just before unstarting the inlet. The pressure signals displayed larger variations after unstart as indicated by the increased levels of the normalized standard deviations. The mean of the time-accurate pressure data also changes significantly after the unstart as the pressure across the inlet is redistributed. The increase in normalized standard deviation indicates that the actual magnitude of the fluctuations is significantly larger for the unstarted inlets than seen when the inlet was operating at maximum back-pressure because of the overall lower mean pressure levels within the unstarted inlets.

For most inlet configurations, examination of the time histories after inlet unstart does not reveal any periodic behavior and the power spectra show a distribution of energy over a wide band of frequencies. However, for one configuration, at the highest contraction ratio (cowl angle = +6 deg), the inlet flowfield displayed an oscillatory behavior after unstart. To illustrate this behavior, the power spectra of the signal from gauge no. 4 (located near the leading edge of the cowl) are shown when the inlet is operating at maximum back-pressure and just after inlet unstart in Fig. 11. A number of closely positioned spikes occur in the spectrum of the unstarted signal around 300 Hz. This indicates that much of the power of the signal resides at these frequencies. This has been confirmed by examination of the autocorrelation of the signal. The autocorrelation of the signal from gauge no. 4 after unstart is shown in Fig. 12. The pattern is characteristic of two periodic signals of nearly identical frequencies interfering with one another at frequencies around 300 Hz. Although the cause(s) behind such driving mechanism(s) for such measured distinct frequencies are unknown, analysis shows that the physical dimension of the model and the flowfield conditions within the unstarted inlet can create a resonant frequency near 300 Hz. The calculated frequency can be determined by using double the physical length between the inlet cowl leading edge and the exit throat of the throttling device (i.e., approximately 27.50 or 55 in., 139.70 cm, for the total out-and-back dis-

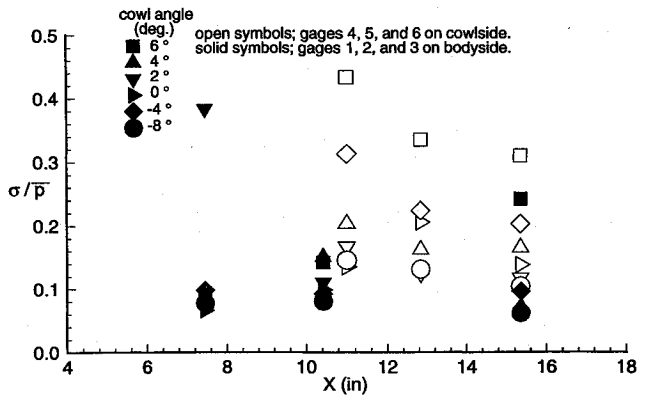

Fig. 10 Normalized standard deviation of the fluctuating pressure signals for each configuration after back-pressure induced inlet unstart.

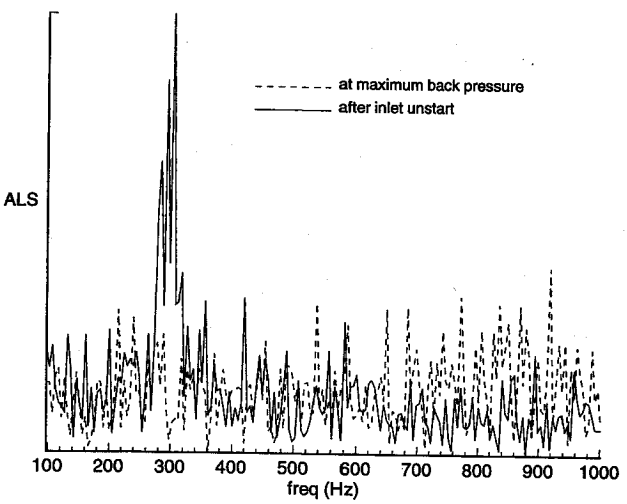

Fig. 11 Power spectra for gauge no. 4, cowl at +6 deg, at maximum back-pressure and after inlet unstart (ALS, arbitrary linear scale).

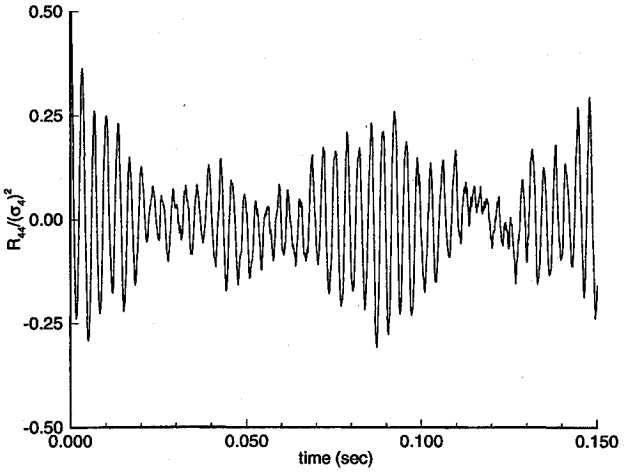

Fig. 12 Autocorrelation for gauge no. 4, cowl at +6 deg, after inlet unstart.

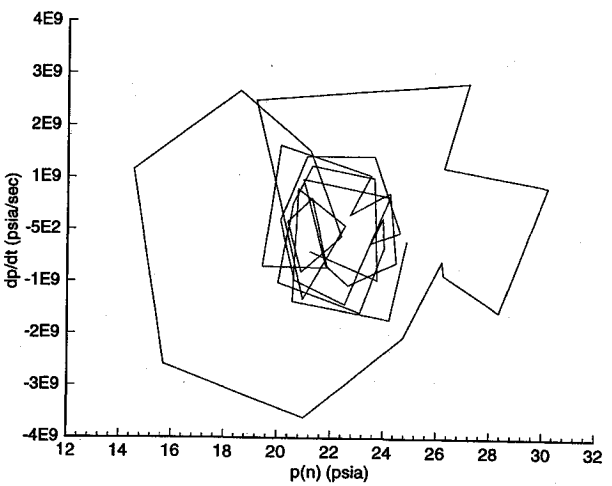

Fig. 13 Phase plane plot of gauge no. 6, cowl at 0 deg, after inlet unstart.

tance), and the speed of sound propagating within the flowfield. Assuming that the sound is propagating most quickly within the warmer air within the boundary layer and that the boundary-layer temperature is approximately the flow total temperature, the propagating speed of sound would be 1128 ft/s (343.80 m/s). The combination of the foregoing specified length and speed of the sound renders a calculated characteristic frequency of 246 Hz.

For every case where the unstarted inlet did not show a dominant frequency of oscillation, examination of the pressure signals has found a deterministic character in the unsteady data. Figure 13 shows a representative plot of the local time derivative of pressure vs the instantaneous pressure value after inlet unstart for 50 sequential data points for the cowl at 0 deg. The curve illustrates an underlying relationship between the instantaneous pressure and its time derivative. This can be easily seen by following the line around the plot and observing the rotational behavior of the distribution. This rotation indicates a deterministic structure indicating a predictive behavior of the unsteady signal. A cross section of this curve can be created by plotting $p(n + 1)$ vs $p(n)$ for some index value n when the time derivative of pressure equals a given constant. This cross section, called a Poincaré map, indicates that the data do not simply repeat the same path as would occur with a simple linear process. (Such an analysis is commonly used to classify dynamic behavior.[14]) However, the points on the cross section do remain grouped together with specific regions clearly preferred by the data and other regions clearly avoided. It is difficult to determine whether this behavior is the result of noisy measurements of a nonlinear process or some type of chaotic behavior of the flowfield. In either case, the deterministic character of the data could possibly be used to limit or reduce the unsteadiness of the pressure field.

Pressure Behavior After Cowl-Induced Unstart

The second type of inlet unstart studied was that induced by the cowl, and labeled the cowl-induced unstart. During these tests, the throttling device was fully open and the back-pressure was not increased in the model. Instead, the cowl was positioned at a shallow angle (e.g., −8 deg) to facilitate inlet starting, and then the included angle between the body and the cowl angle was increased until the inlet unstarted. This type of unstart is because of the high internal contraction ratio of the inlet. For this inlet, the cowl-induced unstart occurred at a cowl angle of 6.5 deg (±0.2 deg).

For large cowl angles, the cowl shock produces two types of shock-wave/boundary-layer interactions. First, a glancing interaction is produced as the cowl shock sweeps across the boundary layer formed along the inlet sidewall. Second, an impinging shock interaction is created when the cowl shock intersects the boundary layer formed along the bodyside of the inlet. The cowl angle at unstart is greater than that predicted by Korkegi's semi-empirical correlations for the incipient separation condition for glancing shock interactions and impinging shock interactions.[15] (For this inlet, a +6.5-deg cowl angle corresponds to a local flow turning angle of +14.5 deg across the cowl shock.) This indicates that shock-induced boundary-

Table 2 Comparison of time-accurate pressure results after BPIU and CIU

	Gauge, psia											
	1		2		3		4		5		6	
Unstart	$\bar{p}$	σ	$\bar{p}$	σ	$\bar{p}$	σ	$\bar{p}$	σ	$\bar{p}$	σ	$\bar{p}$	σ
BPIU	7.03	0.64	7.78	1.10	11.72	2.83	24.05	10.42	9.67	3.24	10.86	3.36
CIU	7.71	1.16	8.60	1.87	12.24	4.73	23.17	15.44	9.15	3.91	11.12	4.20

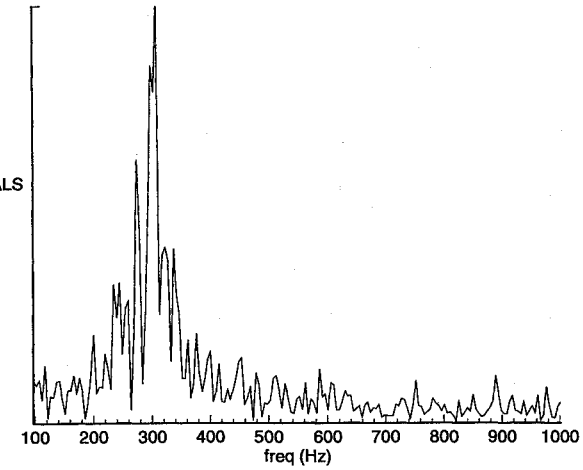

Fig. 14 Power spectra for gauge no. 4 after cowl-induced inlet unstart (ALS, arbitrary linear scale).

layer separation was present, from both types of interactions, before inlet unstart.

The cowl angle when the unstart occurred is very close to the maximum cowl angle examined during the tests with back-pressure. Examination of the mean and fluctuating pressure data revealed similar pressure fields after the back-pressure-induced unstart of the cowl at the +6-deg configuration and after the cowl-induced unstart. However, the mean pressure distributions and the average of the fluctuating pressure measurements after unstart were slightly higher in magnitude for the cowl-induced unstart. In addition, the normalized standard deviation of the time-accurate pressure signals were significantly greater in magnitude for the cowl-induced unstart. A comparison of the results from the time-accurate data for the +6-deg back-pressure-induced unstart and the cowl-induced unstart is shown in Table 2.

Examination of the fluctuating pressure data revealed similar oscillatory behavior after both the back-pressure-induced unstart and the cowl-induced unstart. Figure 14 shows the power spectrum of the pressure signal measured at gauge no. 4 after inlet unstart. Much of the power in the signal is contained near 300 Hz. This spectrum can be compared to the spectrum presented earlier of the gauge no. 4 signal from the +6-deg cowl configuration after back-pressure-induced unstart (Fig. 11). While both of these configurations produce global oscillatory behavior, the magnitude of the oscillations is somewhat greater for the +6-deg cowl, back-pressure-induced unstart case.

Concluding Remarks

The current research focuses on analysis of time-accurate pressure measurements made within the inlet portion of an unfueled dual-mode ramjet/scramjet engine configuration. These measurements were obtained using high-frequency response pressure transducers. In addition, mean surface pressure distributions were measured using conventional surface pressure taps. A throttling device, attached to the rear of the inlet model, was used to simulate the increased inlet back-pressure induced by combustion.

The model incorporated a movable cowl, permitting a number of cowl positions (i.e., contraction ratios) and unstart scenarios to be studied. One scenario was to position the cowl at the desired test angle from −8 to +6 deg, relative to the free-stream direction, and then use a throttling device to increase the inlet back-pressure until unstart occurred. The time-accurate measurements were analyzed at the conditions of maximum permissible back-pressure and after inlet unstart. In the second scenario, the cowl angle was increased during a run until a cowl-induced unstart occurred. Mean and time-accurate data were analyzed after the unstart. The major conclusions of this study are as follows:

1) Increasing the inlet back-pressure increased the normalized standard deviation of the pressure signals.

2) The inlet contraction ratio has a major impact on both the time-accurate and mean pressure measurements at maximum back-pressure.

3) Inlet unstart appears as a high-pressure wave moving upstream through the inlet at a velocity from 182–230 ft/s.

4) The unstarted inlets displayed a major redistribution of the pressure field and increased levels of pressure fluctuations.

5) The −8- to +4-deg cowl configurations did not indicate an oscillatory behavior after unstart, but did demonstrate some deterministic characteristics.

6) The +6-deg cowl configuration displayed an oscillatory behavior after unstart with most of the power in the signal located around 300 Hz.

7) The cowl-induced unstart occurred at an angle greater than that predicted by earlier-developed correlations for the incipient separation condition in glancing-shock and impinging-shock-induced interactions.

8) The cowl-induced, unstarted flowfield displayed similar oscillatory behavior as the +6-deg cowl configuration after back-pressure-induced unstart, with most of the signal's power centered around 300 Hz.

Acknowledgments

The assistance of and discussions with Earl Andrews of NASA Langley are gratefully acknowledged. Assistance during the wind-tunnel experiments is also acknowledged from Troy Middleton of NASA Langley and Technicians Kim Stroupe and Clint Reese.

References

[1]Billig, F. S., "Propulsion Systems from Takeoff to High-Speed Flight," *High-Speed Flight Propulsion Systems*, edited by S. N. B. Murthy and E. T. Curran, Progress in Astronautics and Aeronautics, AIAA, Washington, DC, 1991, pp. 21–100.

[2]Key, I., Peschke, W. T., and Guile, R. N., "Hydrocarbon-Fueled Scramjet Combustor Investigation," *Journal of Propulsion and Power*, Vol. 8, No. 2, 1991, pp. 507–512.

[3]Curran, E. T., and Stull, F. E., "The Utilization of Supersonic Combustion Ramjet Systems at Low Mach Numbers," Aero Propulsion Lab., RTD-TDR-63-4097, Wright–Patterson AFB, OH, Jan. 1964.

[4]Pratt, D. T., and Heiser, W. H., "Isolator-Combustor Interaction in a Dual-Mode Scramjet Engine," AIAA Paper 93-0358, Jan. 1993.

[5]Billig, F. S., Corda, S., and Pandolfini, P. P., "Design Techniques for Dual Model Ram-Scramjet Combustors," *Hypersonic Combined Cycles Propulsion*, CP 479, AGARD, 1990.

[6]Andrews, E. H., Trexler, C. A., and Emami, S., "Tests of a Fixed-Geometry Inlet-Combustor Configuration for a Hydrocarbon-Fueled, Dual-Mode Scramjet," AIAA Paper 94-2817, June 1994.

[7]Hardin, J. C., "Introduction to Time Series Analysis," NASA RP-

1145, March 1986.
[8]Bendat, J. S., and Piersol, A. G., *Random Data*, Wiley, New York, 1986.
[9]Emami, S., Trexler, C. A., Auslender, A. H., and Weidner, J. P., "Experimental Investigation of Inlet-Combustor Isolators for a Dual-Mode Scramjet at a Mach Number of 4," NASA TP-3502, May 1995.
[10]Reddy, D. R., and Weir, L. J., "Three-Dimensional Viscous Analysis of a Mach 5 Inlet and Comparison with Experimental Data," *Journal of Propulsion and Power*, Vol. 8, No. 2, 1992, pp. 432–440.
[11]Dolling, D. S., "Fluctuating Loads in Shock Wave/Turbulent Boundary Layer Interaction: Tutorial and Update," AIAA Paper 93-0284, Jan. 1993.
[12]Zorumski, W. E., "Fluctuating Pressure Loads Under High Speed Boundary Layers," NASA TM-100517, Oct. 1987.
[13]Wieting, A. R., "Exploratory Study of Transient Unstart Phenomena in a Three-Dimensional Fixed-Geometry Scramjet Engine," NASA TN D-8156, March 1976.
[14]Wiggins, S., *Introduction to Applied Nonlinear Dynamical Systems and Chaos*, Springer–Verlag, New York, 1990.
[15]Korkegi, R. H., "Comparison of Shock-Induced Two- and Three-Dimensional Incipient Turbulent Separation," *AIAA Journal*, Vol. 13, No. 4, 1975, pp. 534, 535.